15th International Conference on Greenhouse Gas Control Technologies, GHGT-15

15th 18th March 2021 Abu Dhabi, UAE

Modelling the DAS response for offshore CO_2 storage sites

Vincent Vandeweijer[a]*, Bob Paap[a], Arie Verdel[a], Rob Mellors[b], Alan F. Baird[c], Anna L. Stork[d], Antony Butcher[c]

[a]TNO Applied Geosciences, Princetonlaan 6, 3584CB Utrecht, Netherlands
[b]Lawrence Livermore National Laboratory, 7000 East Avenue, Livermore, CA USA
[c]School of Earth Sciences, University of Bristol, Queens Rd, Bristol BS8 1RJ, UK
[d]Silixa Ltd., 230 Centennial Park, Centennial Avenue, Elstree WD6 3SN, UK

Abstract

Using fiber-optic cables as distributed sensors to monitor the subsurface is one of the fastest growing acquisition technologies in the hydrocarbon energy sector. Since the first exploration and production downhole field trial of a Distributed Acoustic Sensing (DAS) system for seismic monitoring in 2009, the technology has boomed. It has already proven to be an effective tool for acquiring vertical seismic profiles (VSP), performing passive interferometric measurements, and monitoring of microseismic earthquakes.

DAS cables record seismo-acoustic wavefields and ground motions because ground-motion-induced changes in strain on the fiber affect the phase of back-scattered light in the fiber. Commercially available systems already provide sub-meter spatial resolution in sensing fibers up to 50 km in length with a frequency response up to several kHz. This exceeds the frequency range and spatial coverage of conventional seismic sensors. As a result, surface and borehole monitoring with DAS in addition to traditional sensors will most likely form a central component of future Measurement, Monitoring and Verification (MMV) systems for CO_2 storage.

DAS, however, does possess some key disadvantages in that it only provides a single component measurement which is most sensitive to motions in line with the fiber. DAS also measures linear strain rather than particle motion, meaning the recorded signals are not directly comparable to conventional sensors. In order to better understand the response of DAS it is therefore necessary to understand the seismic source, path, site and instrument effects.

The ACT DIGIMON project aims to develop and demonstrate an affordable, flexible and societally embedded Digital Monitoring early-warning system, for monitoring CO_2 storage sites. Within the DIGIMON concept fiber-optic monitoring will form a key component, therefore a thorough understanding of the response of DAS systems, including the transfer function, is a fundamental issue to be addressed.

In this paper we present our modeling approach for the DAS response for a fictive CO_2 storage site. The workflow exploits geometrical models of different complexity which in the end are representative of North Sea geology. Using ray tracing techniques and the seismic waveform modelling packages: SW4 and SPECFEM3D, we were able to analyze and compare these modeling approaches in relation to the response of a DAS system. With varying model complexity, we accurately capture and analyze the DAS response for realistic cable geometries. These geometries represent both vertical and horizontal deployments, which replicate fiber placed in wells and deployed on the seabed and or in shallow trenches.

Keywords: Offshore CO_2 storage sites; DAS response; DAS transfer function; Seismic modelling; SW4; SPECFEM3D

* Corresponding author. *Tel.*: +31-6-11700457, *E-mail address:* vincent.vandeweijer@tno.nl

1. Introduction

Monitoring forms an important component of CO_2 geological storage projects. Seismic monitoring in particular plays a crucial role in characterizing the site before injection, demonstrating conformance with agreed operational conditions and verifying CO_2 containment both during and after injection. 3D surface seismic surveys and Vertical Seismic Profiles (VSPs) are used to track the movement of the CO_2 plume and understand the geomechanical effects of injection. Additionally, microseismic monitoring can be deployed to understand the seismic hazard associated with a project and to monitor pressure effects and fluid movement because the activation of faults and fractures could result in a breach of CO_2 containment. Recent developments in fiber-optic monitoring technology have facilitated the use of Distributed Acoustic Sensing (DAS) in seismic applications and the potential for the technology is only now beginning to be realized.

DAS makes use of optical time domain reflectometry (OTDR) principles to detect seismic waves incident on a fiber-optic cable. DAS interrogators emit pulses of laser light into a fiber and measure the Rayleigh backscattered light resulting from variations in refractive index along a fiber. A DAS system can record the full wavefield amplitude and phase at every point along the fiber over a wide range of frequencies with a large dynamic range. Changes in strain on the fiber due to the passage of seismic wave fronts result in changes in the recorded signal and interrogators can measure changes in axial strain down to sub-nano strain resolution [1]. DAS systems are able to record data on cables up to tens of km long and with a spatial sampling <1m with recording frequencies up to 100 kHz. The systems have a broadband frequency response [2], exceeding the range provided by conventional seismic sensors. The range of measurements possible with DAS make them an attractive option for seismic monitoring, including for geological CO_2 storage. However, some aspects of DAS, for example the single component nature of the measurement, are barriers to the uptake of the technology. A better understanding of the strain or strain-rate data recorded by the systems will help to overcome these barriers with new developments in seismic processing.

DAS has proven to be an effective tool for acquiring VSPs [3], [4] and has been used to monitor the extent of the CO_2 plume at the Aquistore CCS project [5]. The prospect of multiple applications for the technology make it a flexible and cost-effective option for monitoring. Recently DAS has been successfully applied to microseismic monitoring [6], [7], [8] and, when combined with slow strain measurements, it provides information on fracture propagation and fluid movement [9]. Additionally, DAS data has been used to image the subsurface using seismic interferometry [10]. Fiber-optic cables are often permanently installed and therefore repeatable and on-demand interferometry surveys can be conducted without the need for mobilization active seismic sources. The technology is also being investigated for use in surface seismic surveys.

To understand the response of DAS it is necessary to understand (1) the seismic source, (2) the path effects and (3) the site and instrument effects. In this paper we discuss the modelling of the first two contributions of the DAS response; the source and path effects. We simulate the resulting particle motion and strain at the fiber location, resulting from realistic microseismic sources in geological models representative of the North Sea. The third aspect, site and instrument effects, accounted for in the form of a transfer function are being further investigated as part of the ACT DigiMon project.

2. Models

2.1. Modelling software

Of the many software options available for simulating seismic wave propagation, we choose two popular open-source software packages to include in our test: SW4 and SPECFEM3D Cartesian. SW4 [11], [12] uses a node based finite difference approach to solve the seismic wave equations to fourth-order accuracy. SPECFEM3D [13], [14] uses the spectral element method. Both of these packages are commonly used to model particle motion as measured on conventional seismometers. We are not aware of any examples where they have been applied to model DAS datasets. Additionally, for the more simple models we apply analytical and semi analytical modelling approaches (e.g. ray-theory and wavenumber integration methods) for benchmarking purposes.

2.2. Modelling approach

A three-stage approach is adopted to assess the suitability of the modelling programs and refine the selection of model parameters. Initially, a simple homogeneous model is used to compare the synthetics produced by the different software packages. This allowed for identification of the causes of inconsistencies between the models, and once remedied we gradually increased the complexity of the model.

The three stages proposed in this modelling approach are:

1. Homogeneous medium; using a moment tensor source. This can also be compared with analytical methods (e.g. ray theory).
2. Three-Layer model with force source. Layers are homogeneous (no velocity gradient). This will allow a comparisons involving reflections/transmissions at interfaces, as well as surface waves.
3. More complex North Sea model; after consistent results have been generated from the two previous stages and the velocity model has been finalized.

2.3. Geological North Sea model

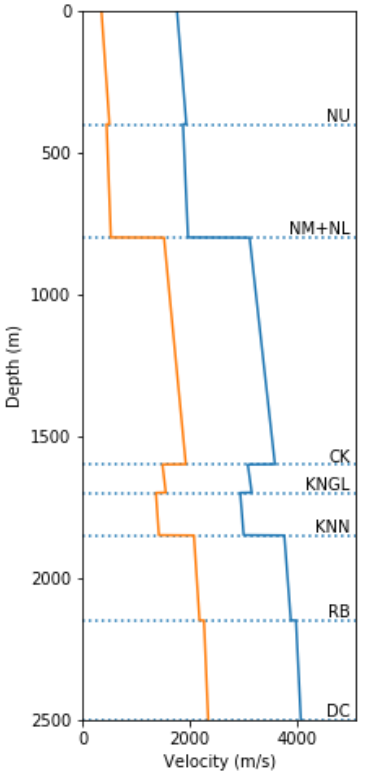

Figure 1. A representative North Sea velocity model, based on VELMOD-3 [15]. Vp (blue line) and Vs (orange line), including the names of the Groups and Formations. NU, NM and NL represent the Upper, Middle and Lower North Sea Group sediments, CK – Upper Chalk, KNGl and KNN – Lower Chalk Group, RB, represents Triassic sediments and finally DC some Carboniferous strata.

For the generic geologic model representative of the North Sea we used data from VELMOD-3 [15], which describes a layer cake P-velocity model of the Dutch North Sea, based on a compilation of velocity data from a wide range of geologic units. The P-wave velocity of most of the geological units is described by a simple linear function

$$V(z) = V_0 + kZ,$$

where V is the velocity at depth Z, V_0 is the "normalized velocity", and k is the velocity depth gradient. V_0 and k are determined empirically by linear regression of velocity-depth data.

This parameterization makes it easy to generate simple 1D P-wave velocity models for an arbitrary selection of stratigraphic layers. However, the model does not include S-wave velocities. To estimate these, we adopt empirical relationships between P- and S-wave velocities for sedimentary rocks given by Castagna et al. [16]. Figure 1 shows an example 1D model generated following this methodology. Note that for actual site-specific models, the velocity model would be better derived using sonic-velocity and density logs from actual borehole data.

3. Results

3.1. Homogeneous model

For initial testing a homogeneous velocity model was used. We used a homogeneous velocity and density model with a Vp of 1966.76 m/s, a Vs of 646.45 m/s and a density of 1960 kg/m^3. Absorbing boundary conditions were used for all boundaries and we activated channels in a vertical array with a 10 meter interval. The source had an offset to the array and was placed at a depth of 700 m. and we used a gaussian displacement wavelet with central frequency of 7 Hz.

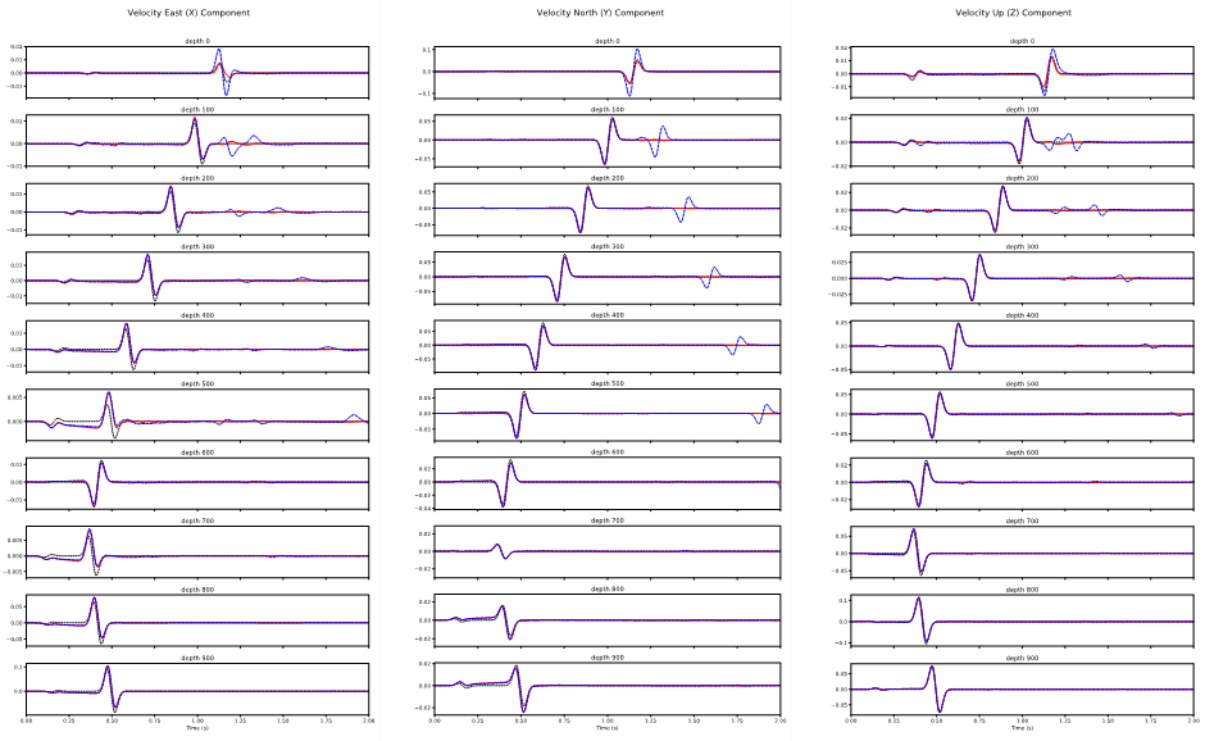

Figure 2. Comparison of synthetic particle-velocity waveforms for the homogeneous model computed using SPECFEM3d (red solid line), SW4 (blue dashed line) and Ray-theory synthetics (dotted black line).

For this homogeneous simulation, synthetics were also produced using ray-theory to provide an analytical solution to compare with. Figure 2 shows a comparison of the particle velocity synthetics for every 10th receiver in the vertical array (100 m spacing). The three models produce very consistent results except for a few key differences. There is an inconsistency in the amplitudes in the SW4 synthetics at the shallowest receiver (depth=0m), which is due to the SW4 model using a free surface boundary condition at the top interface instead of the prescribed absorbing boundary condition. This introduces amplitude differences at the surface as well as a reflected wave propagating downwards, which is not seen in the SPECFEM3D and ray-synthetics. Additionally, the ray synthetics show a small difference in amplitude between the P and S arrivals at receivers close to source depth (most clearly seen on the X component of

receivers 500 and 700 m depth of Figure 2). This is because ray theory synthetics use a far-field approximation to the solution of the wave equation (i.e. there are additional effects near the source that are not accounted for). However, the difference is relatively small, and both SW4 and SPECFEM3D produce consistent results at this depth, which gives us confidence that they are correctly modelling the near field effect.

3.2. Three Layer Model

Next, a simple three layer model was constructed using SPECFEM3D and SW4 using the geometry as shown in Figure 3.

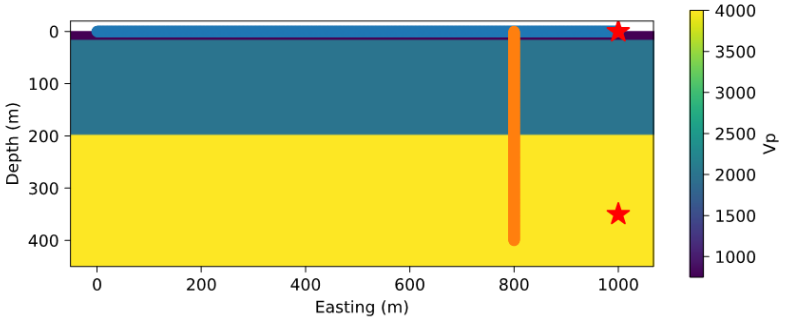

Figure 3. Cross sectional view of three layer model, showing P velocities (background color), source locations (red stars) and array geometry (surface array in blue and vertical array in orange).

For this model, the mesh was generated in SPECFEM3D using an element size of 25 m. This element size is based on guidelines of required element sizes for spectral element models to accurately simulate the smallest estimated wavelengths expected, here corresponding to the S wave velocity in the shallowest and slowest layer. The SW4 model was generated with a grid spacing of 4 m throughout most of the model, but with mesh refinement in the upper layer to achieve a grid spacing of 1 m. This was required to allow a station spacing of 1 m along the surface array, but also has the effect of increasing the accuracy for waves propagating in the shallow layers.

The models generally showed quite good agreement for the body wave arrivals, however the surface waves showed a poorer fit. There was some evidence of grid dispersion in the SPECFEM3D model and there seemed to be some reverberations present in the SPECFEM3D synthetics which were not seen in the SW4 results. This suggests that a smaller element size may be needed in SPECFEM3D to accurately model surface waves and S waves in slower layers.

Results from similar trace comparison of the velocity synthetics for a buried source also match reasonably well, except for some variation towards the corners, suggesting some boundary effects.

For the SPECFEM3D model, strain-rate synthetics were calculated by computing the spatial gradient of the in-line component of the velocity synthetics using 2nd order accurate central differences with 1m channel spacing. For this we followed equation 3 of Wang et al. (2018) [17].

Some undesired side reflections in the SPECFEM3D model could be further reduced by making use of convolutional perfectly matched layer absorbing conditions (CMPL) instead of Stacey absorbing boundary conditions. SW4 outputs strain seismograms directly, and we converted these to strain-rate by applying an additional time derivative. Overall the synthetics using both methods seem to agree reasonably well.

4. The North Sea Model

Finally, a generic “North Sea” model was constructed using the specifications as mentioned in Table 1 and with model geometry as shown in Figure 4.

Table 1. parameters used for the generic "North Sea" model.

Velocity and density model	Receivers	Source parameters
• P-wave velocities were based on Velmod-3 [12] as in figure 1. • S-wave velocities were created from an empirical relationship between P and S velocities [16] • The density was arbitrarily chosen (first 2 layers 1960 kg/m^3, lower layers 2600 kg/m^3)	• The vertical array was located in the middle of the model and channels were placed at a 1m. interval • Two horizontal surface arrays ran N-S and E-W, centered over vertical array (figure 4) • Also with a channel interval of 1m.	• The source was located slightly off the vertical array at a depth of 1630 m. • A gaussian displacement wavelet with central frequency of 7 Hz was used.

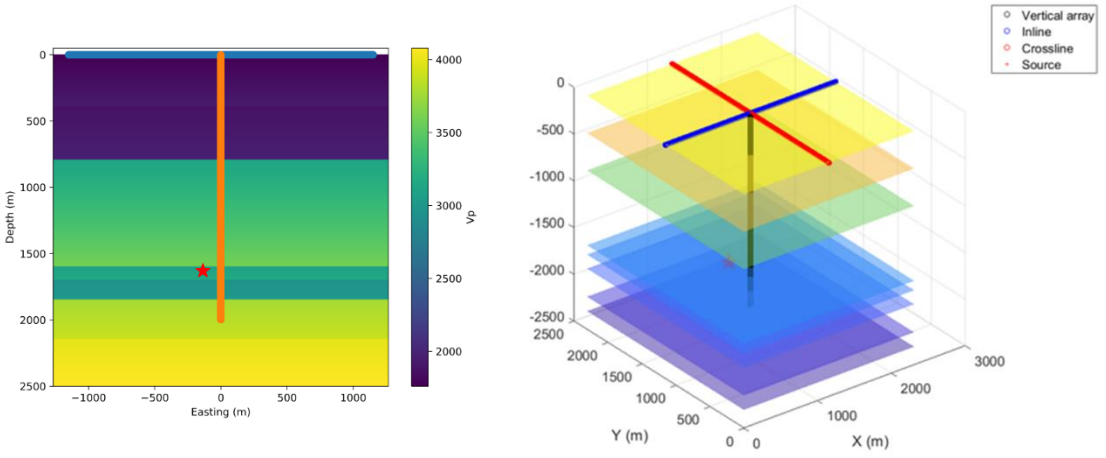

Figure 4. Left: East-West cross section through the North Sea model showing P velocities (background color), source location (red star) and array geometry (E-W array in blue and borehole array in orange). Right: 3D view of the model showing array geometry, and major lithological interfaces of the velocity model.

Initial results showed some significant mismatch between the SW4 and SPECFEM3D results. Figure 5 shows a trace comparison of the vertical velocity synthetics along the upper 1000m of the borehole array. The travel-times between the two models seem to agree, and the amplitudes are the same order of magnitude, however the details of the amplitudes and shape of the waveforms do not match.

One of the possible reasons for the mismatch was that there was insufficient grid resolution for SW4 within the deeper low velocity layers where the source is located. SW4 supports variable mesh size but in a constrained manner. The lowest grid size is set and defined as the lowermost grid. Mesh refinement steps are set which reduce the grid size by half. In this way, for example, a grid size of 8 can be reduced to a surface grid of 2 by two refinement settings. Although this decreases the time need for calculations, two difficulties exist:

1. SW4 receivers must be at mesh nodes. A grid spacing of 8 means that the receivers cannot be closer than 8 meters.
2. The refinement generally assumes that velocities increase with depth and that the points per wavelength does not vary significantly with each layer. The North Sea model has a pronounced low velocity zone which makes a smooth variation of points per wavelength impossible. This may lead to some error.

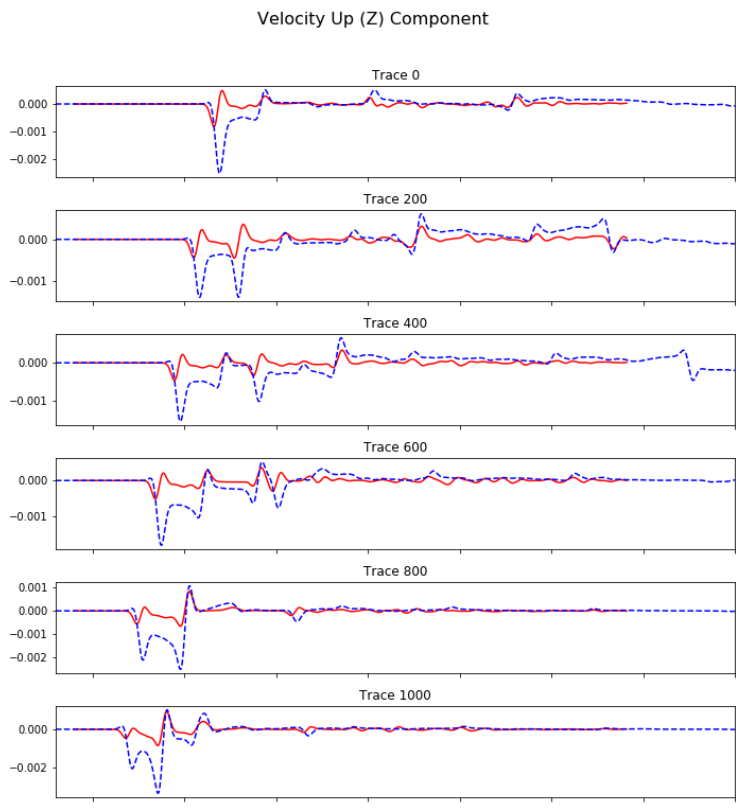

Figure 5. Trace overlay comparisons of in-line velocity synthetics for the North Sea model along the borehole array (Z component). Red lines indicate SPECFEM3D and blue dashed lines indicate SW4. Note the source was located at a depth of 1630m. Note that a revised SW4 model resolved much of the discrepancy between SPECFEM3D and SW4 (see Figure 7).

Figure 6 compares seismograms at the surface for three possible mesh refinement scenarios:

1. Grid spacing of h = 2 m with no grid refinement
2. Grid spacing of h = 4 m at the base, refined to h = 2 m above z=800 m
3. Grid spacing of h = 8 m at the base, refined to h = 4 m and 2 m at 1800 m and 800 m depth, respectively

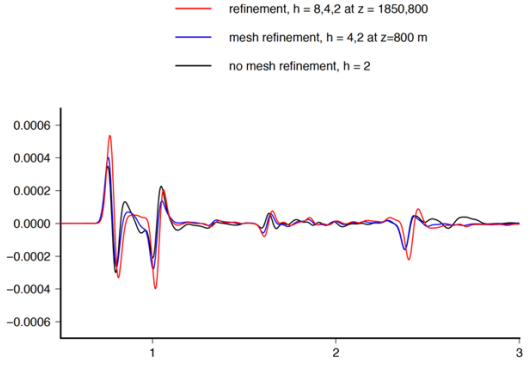

Figure 6. Comparison of seismogram at the surface for three different mesh refinement scenarios.

I/O and hardware constraints may significantly increase the time of computation. For SW4, similar models with different number of receivers differ significantly in required time. One workaround for this is to define different grid specifications for borehole versus surface arrays. A borehole model requires a small grid size at depth to allow for closely spaced receivers. In this case, the horizontal extent may be restricted to ensure a relatively small model. If

surface receivers over a wide extent are needed, then mesh refinement can be used, as the uppermost layer is always the smallest grid size.

Figure 7 shows a trace comparison of the three component velocity synthetics along the borehole array between the SPECFEM3D model and a revised SW4 model with a grid spacing of h=2 m with no grid refinement. The horizontal extent of the model was constrained to allow small model size, surface receivers were not modelled. We saw a greatly improved match between the two models in this scenario. Note, however, that there is some evidence of grid dispersion present in the SPECFEM3D model at shallower (and low velocity) depths. Figure 8 shows the strain-rate synthetics along the full depth of the borehole.

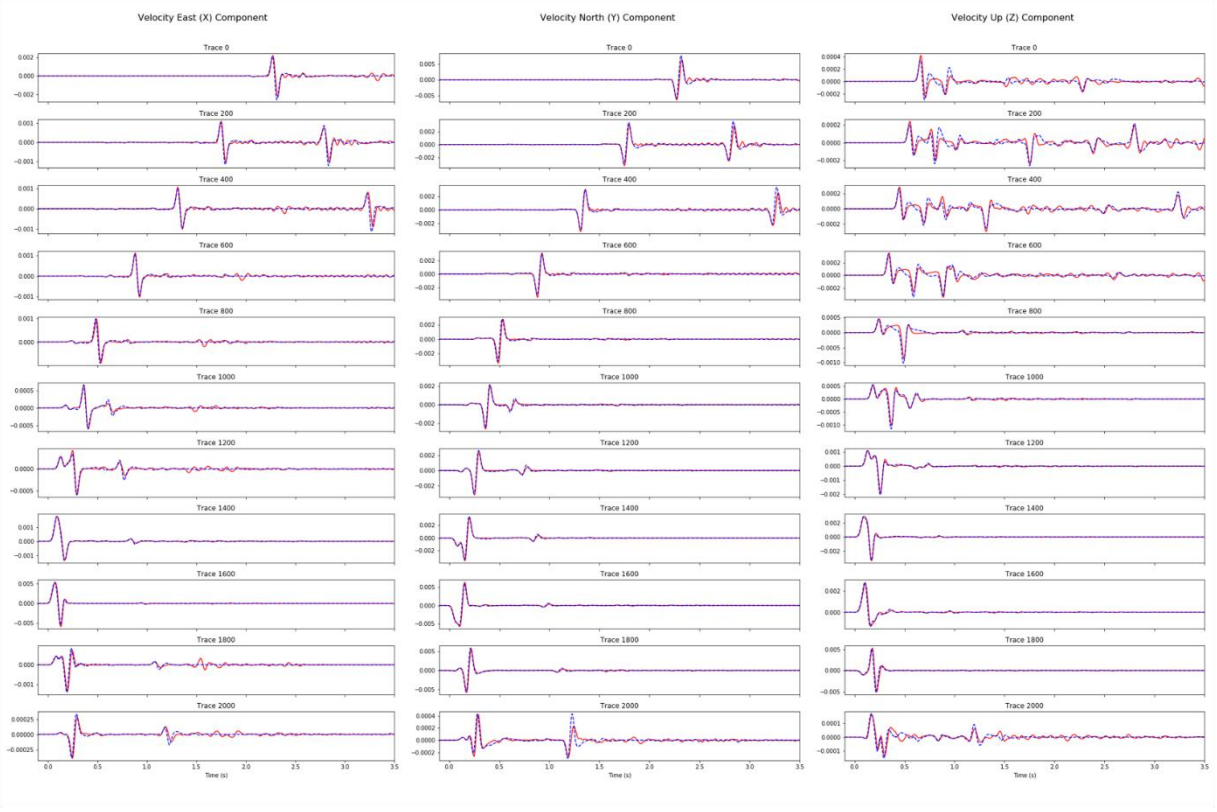

Figure 7. Trace overlay comparisons of 3C velocity synthetics for the North Sea model along the borehole array (E,N and Z components). Red lines indicate SPECFEM3D and blue dashed lines indicate the revised SW4 model with h=2m and no grid refinement. The source was located at a depth of 1630m. There is quite good agreement between the models, however, there appears to be evidence of grid dispersion in the SPECFEM3D model in the shallow receivers.

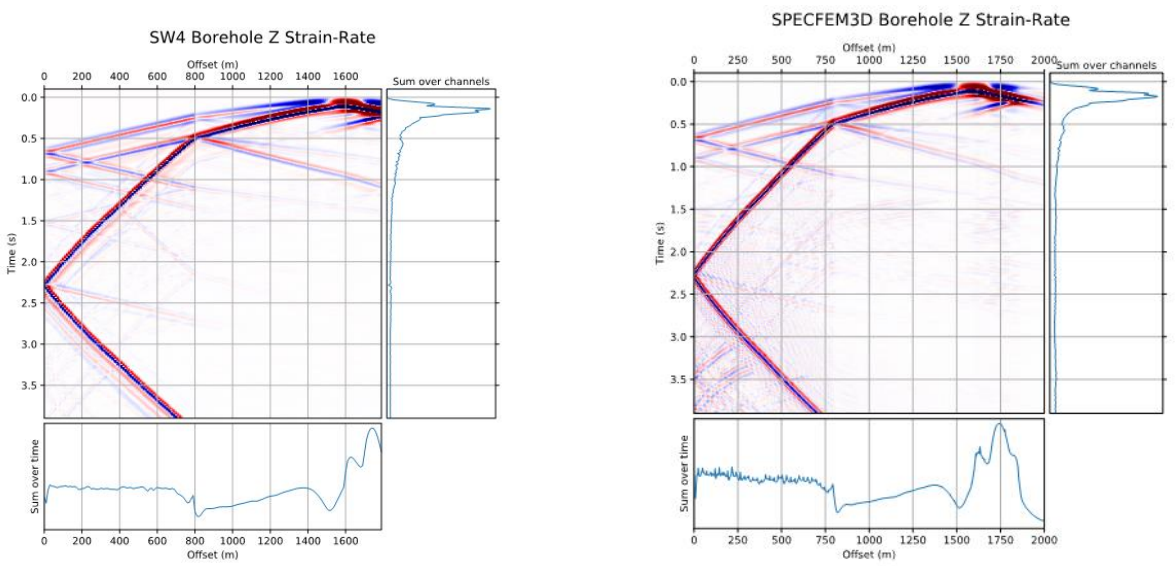

Figure 8. Strain-rate synthetics for the revised North Sea model recorded along the borehole array. Channel 0 is located at the surface, with the base of the array at 2000 m depth. The source is located at a depth of 1630 m.

5. Discussion

For the activities planned within the ACT DIGIMON project it is important to be able to model a reliable DAS response. This capability will ultimately be used to understand and support monitoring operations for offshore CO_2 storage sites via e.g. inversion work flows. Our work investigated the reliability of 2 full waveform modelling packages and an analytic (ray tracing) approach. In future work we will further apply and test these models against actual field data. This will also allow us to delve further into the fundamental issue of transfer function related work relevant to enabling the accurate and efficient monitoring CO_2 storage operations with DAS.

6. Conclusion

Through a series of progressively more complex models we have shown that we can achieve reasonably consistent synthetic DAS datasets using both SW4 and SPECFEM3D. This gives confidence that the wavefields are accurately being modelled, such that either method can be used to create DAS synthetic data for arbitrary subsurface models. This is relevant to design optimal network configurations and to improve our understanding of the response of DAS measurement systems to seismic wavefields, and to correctly interpret observed seismic events. However, through this analysis we identified some differences in the capabilities of each modelling method such that, depending on the use case, one method may offer advantages over the other.

Regarding the array geometry, one of the benefits of DAS systems is that they provide a very dense sampling of the wavefield, with channel spacing in the order of a meter. However, this close spacing presents a challenge for modelling DAS synthetics with SW4, as receivers must be at mesh nodes (e.g. A grid spacing of 8 means that the receivers cannot be closer than 8 meters). In contrast SPECFEM3D allows receivers to be placed at any location within the mesh, allowing for more flexibility in modelled array geometries.

To suppress boundary effects at the lateral sides of the model geometry each model employed a form of absorbing boundary conditions. The SW4 models used supergrid boundaries and the SPECFEM3D models initially used Stacey boundary conditions. The SW4 models outperformed SPECFEM3D in this respect. Clear boundary reflections could be seen in the SPECFEM3D models, which then interferes with other arrivals. However, the boundary conditions of

SPECFEM3D models can be significantly improved by using more sophisticated absorbing boundary conditions like convolutional perfectly matched layer (CPMLs).

One of the major benefits of SW4 over SPECFEM3D is that it supports the direct output of strain seismograms for all 6 independent components of the strain tensor. In contrast, SPECFEM3D supports only the output of 3 component particle motion seismograms, and the conversion to strain must be done through numerical differentiation in post processing. This is not a significant weakness when simulating simple linear fibers, where only the axial strain needs to be modelled. However, there are scenarios where having the full strain tensor output would be desirable, for example in modelling the response of helically wound cables which are sensitive to strain in multiple directions.

Acknowledgements

This paper has been produced with support from the ACT DIGIMON, (project no 299622) which is supported by the ACT2 international initiative http://www.act-ccs.eu/about-us and funded by GASSNOVA (NO), RCN (NO), BEIS (UK), Forschungszentrum Jülich (DE), GSRT (GR), RVO (NL), UEFISCDI (RO), DoE (US), Repsol Norge (NO) and Equinor (NO).

References

[1] Parker, T., S., Shatalin, and M., Farhadiroushan (2014). Distributed acoustic sensing – A new tool for seismic applications: First Break, 32, 61–69, doi: https://doi.org/10.3997/1365-2397.2013034.

[2] Lindsey, N. J., Rademacher, H., & Ajo-Franklin, J. B. (2020). On the broadband instrument response of fiber-optic DAS arrays. Journal of Geophysical Research: Solid Earth, 125, e2019JB018145. https://doi.org/10.1029/2019JB018145

[3] Harris, K., D. White, D. Melanson, C. Samson and T.M. Daley (2016). Feasibility of time-lapse VSP monitoring at the Auistore CO_2 stroage site using a distributed acoustic sensing system, Int. J. Grennshouse Gas Cont., 50 248-260, doi:10.1016/j.ijggc.2016.04.016.

[4] Correa, J., B. M. Freifeld, M. Robertson, R. Pevzner, A. Bona, D. Popik, S. Yavuz, K. Tertyshnikov, S. Ziramov, V. Shulakova, and T. M. Daley (2017). Distributed acoustic sensing applied to 4D seismic-preliminary results from the CO_2CRC Otway site field trials: 79th Annual International Conference and Exhibition, EAGE, Extended Abstracts, Tu A1 15, doi: 10.3997/2214-4609.201700811.

[5] Harris, K., D. White, and C. Samson (2017). Imaging the Aquistore reservoir after 36 kilotonnes of CO_2 injection using distributed acoustic sensing: Geophysics, 82, no. 6, M81–M96, doi: 10.1190/geo2017-0174.1.

[6] A. L. Stork, A. F. Baird, S. A. Horne, G. Naldrett, S. Lapins, J.-M. Kendall, J. Wookey, J. P. Verdon, A. Clarke, and A. Williams, "Application of machine learning to microseismic event detection in distributed acoustic sensing data," Geophysics 85(5), KS149–KS160 (2020).

[7] Verdon, J. P., S. A. Horne, A. Clarke, A. L. Stork, A. F. Baird, and J.-M. Kendall, 2020,Microseismic monitoring using a fiber-optic distributed acoustic sensor array: GEOPHYSICS, 85, no. 3, KS89-KS99.

[8] Walter, F., Gräff, D., Lindner, F. et al. Distributed acoustic sensing of microseismic sources and wave propagation in glaciated terrain. Nat Commun 11, 2436 (2020). https://doi.org/10.1038/s41467-020-15824-6

[9] Richter P., T. Parker, C. Woerpel, W. Wu, R. Rufino and M. Farhadiroushan (2019). High-resolution Distributed Acoustic Sensor using engineered fiber for hydraulic fracture monitoring and optimization in unconventional completions, SEG International Exposition and 89th Annual Meeting, 4874-4878, DOI: 10.1190/segam2019-3215860.1.

[10] Dou, S., N. Lindsey, A. M. Wagner, T. M. Daley, B. Freifeld, M. Robertson, J. Peterson, C. Ulrich, E. R. Martin, and J. B. Ajo-Franklin (2017). Distributed acoustic sensing for seismic monitoring of the near surface: A traffic-noise interferometry case study: Scientific Reports, 7, 11620, doi: 10.1038/s41598-017-11986-4.

[11] Sjögreen, B., and Petersson, N. A. A fourth order accurate finite difference scheme for the elastic wave equation in second order formulation. Journal of Scientific Computing 52, 1 (2012), 17–48.

[12] Petersson, N. A., and Sjögreen, B. High order accurate finite difference modeling of seismo-acoustic wave propagation in a moving atmosphere and a heterogeneous earth model coupled across a realistic topography. Journal of Scientific Computing 74, 1 (2018), 290–323.

[13] Komatitsch, D., and Tromp, J. Introduction to the spectral element method for three-dimensional seismic wave propagation. Geophysical journal international 139, 3 (1999), 806–822.

[14] Tromp, J., Komattisch, D., and Liu, Q. Spectral-element and adjoint methods in seismology. Communications in Computational Physics 3, 1 (2008), 1–32.

[15] Pluymaekers, M. P. D., Doornenbal, J. C., and Middelburg, H. Velmod-3.1. Tech. Rep. R11014, TNO, 2017.

[16] Castagna, J.P., Batzle, M.L. & Eastwood, R.L. Relationships between compressional-wave and shear-wave velocities in clastic silicate rocks. Geophysics, 50, 571–581, 1985.

[17] Wang, H. F. et al. Ground motion response to an ml 4.3 earthquake using colocated distributed acoustic sensing and seismometer arrays. Geophys. J. Int. 213, 2020–2036 (2018).